RADC-TR-71-245
TECHNICAL REPORT
NOVEMBER 1971

LASER RADAR CROSS-SECTION AND REFLECTIVITY MEASUREMENTS AT .48, .63, AND 10.6 MICRONS

Approved for public release;
distribution unlimited.

Rome Air Development Center
Air Force Systems Command
Griffiss Air Force Base, New York

When US Government drawings, specifications, or other data are used for any purpose other than a definitely related government procurement operation, the government thereby incurs no responsibility nor any obligation whatsoever; and the fact that the government may have formulated, furnished, or in any way supplied the said drawings, specifications, or other data is not to be regarded, by implication or otherwise, as in any manner licensing the holder or any other person or corporation, or conveying any rights or permission to manufacture, use, or sell any patented invention that may in any way be related thereto.

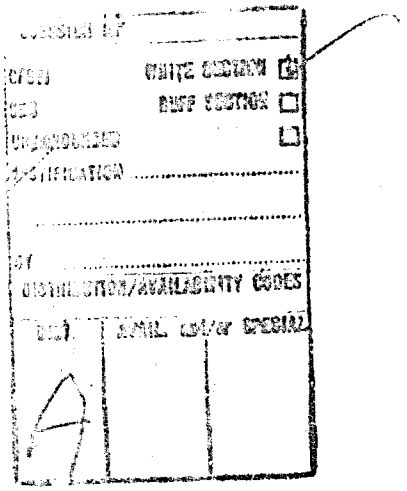

Do not return this copy. Retain or destroy.

LASER RADAR CROSS-SECTION AND REFLECTIVITY MEASUREMENTS AT .48, .63, AND 10.6 MICRONS

Fred J. Demma
James H. Michels

FOREWORD

This effort was accomplished under Job Order Number 65270000, in-the-house funds.

The authors acknowledge many helpful discussions with their RADC colleagues, Messrs. Frank J. Rehm and Daniel Tauroney.

This report has been reviewed by the Information Office, OI, and is releasable to the National Technical Information Service (NTIS).

This technical report has been reviewed and is approved.

Approved: ARTHUR J. FROHLICH
Chief, Techniques Branch
Surveillance & Control Division

Approved: LEO M. SULLIVAN
Colonel, USAF
Chief, Surveillance & Control Division

FOR THE COMMANDER:
IRVING J. GABELMAN
Chief, Plans Office

UNCLASSIFIED

Security Classification

DOCUMENT CONTROL DATA - R & D

(Security classification of title, body of abstract and indexing annotation must be entered when the overall report is classified)

1 ORIGINATING ACTIVITY (Corporate author) Rome Air Development Center (OCTA) Griffiss Air Force Bae, New York 13440	2a. REPORT SECURITY CLASSIFICATION UNCLASSIFIED 2b. GROUP N/A

3 REPORT TITLE

LASER RADAR CROSS-SECTION AND REFLECTIVITY MEASUREMENTS AT .48, .63, and 10.6 MICRONS

4 DESCRIPTIVE NOTES (Type of report and inclusive dates)

In-House Report

5. AUTHOR(S) (First name, middle initial, last name)

Fred J. Demma
James H. Michels

6 REPORT DATE	7a. TOTAL NO. OF PAGES	7b. NO. OF REFS
November 1971	36	4

8a. CONTRACT OR GRANT NO.	9a. ORIGINATOR'S REPORT NUMBER(S)
N/A Job Order No. 65270000	RADC-TR-71-245 9b. OTHER REPORT NO(S) (Any other numbers that may be assigned this report)

10 DISTRIBUTION STATEMENT

Approved for public release; distribution unlimited.

11. SUPPLEMENTARY NOTES	12. SPONSORING MILITARY ACTIVITY
Fred J. Demma (OCTA) AC 315 330-4305	Rome Air Development Center (OCTA) Griffiss Air Force Base, New York 13440

13. ABSTRACT

The effect of target surface and shape, on the power reflected from it, as a function of aspect angle θ, has been investigated at .48, .63, and 10.6μ in a laboratory environment. In particular, at 48μ the reflected wave amplitude was measured relative to a standard cross section target, a Lambertian Reflector. This enabled the determination of actual Laser Radar Cross Section (LRCS) values for these targets. Further, the experimental results obtained were found to agree closely with analytical predictions based on specular scattering theory.

DD FORM 1 NOV 65 1473

UNCLASSIFIED

Security Classification

UNCLASSIFIED
Security Classification

14 KEY WORDS	LINK A		LINK B		LINK C	
	ROLE	WT	ROLE	WT	ROLE	WT
Laser Radar Lambertian Reflection						

UNCLASSIFIED
Security Classification

GAO--Griffiss AFB NY 1 Dec 1-10

ABSTRACT

The effect of target surface and shape, on the power reflected from it, as a function of aspect angle θ, has been investigated at .48μ, .63μ, and 10.6μ in a laboratory environment. In particular, the experimental results as a function of wavelength correlated very well with accepted roughness scale approximations to specular scattering theory. In addition, at .48μ the reflected wave amplitude was measured relative to a standard cross-section target, a Lambertian Reflector. This enabled the determination of actual Laser Radar Cross Section (LRCS) values for these targets.

TABLE OF CONTENTS

LIST OF FIGURES

LIST OF TABLES

I. INTRODUCTION

An Optical Radar (OR) possessing a high precision angle tracking and discrimination capability, can be a unique diagnostic sensor for interrogating and identifying aircraft and space vehicles at long ranges. However, in order to provide an OR with discrimination/identification capability, information is required about a number of target characteristics, such as the variation of Laser Radar Cross Section (LRCS) with aspect angle θ. As an OR tracks a moving vehicle through a range of aspect angles, the amplitude of the tracking signal will vary in accordance with the change of target cross section with aspect angle. If this amplitude variation could be identified with a previously found correlation between a known target's surface/shape and its measured variation of LRCS with angle, it could lead to a partial solution of the target discrimination problem. Thus, if LRCS vs θ information is provided by an OR, and is properly combined with other information characteristic of the target such as its doppler spectrum, [1] a target signature will result and can be utilized as a discriminant.

In order to investigate the effect of a target's surface and shape on the power reflected from it as a function of θ, a laboratory measurement program was initiated.

Various curved and flat shapes were utilized with different surface finishes. Also, the reflected power measurements were made at different wavelengths for comprehensive purposes and to enable a comparison with analytical estimates independent of wavelength. This report presents some unique laboratory measurements which are to be regarded as preliminary, pending additional measurements utilizing new equipments whose need was uncovered by this present investigation. These additional measurements will be made at an outdoor model range in close proximity to a 10μ OR. This will provide in-depth data on target characteristics of importance to the radar while being in the same physical environment.

II. EXPERIMENTAL SETUP

This section discusses the experimental arrangements that were utilized to investigate the power reflected from various shaped and finished targets, as a function of aspect angle, at a number of wavelengths.

The specific targets used were a flat gold coated mirror, two convex gold coated mirrors 3.81 cm in diameter with 10 cm and 20 cm radii of curvature, and two cylinders 2 cm by 2 cm, one nickel plated and the other silver foiled. In addition, the wavelengths used to illuminate these targets were .48μ (Argon),

.63μ (HeNe), and 10.6μ (CO_2). A schematic diagram of the reflected power measuring system is shown in Figure 1 and a photograph of the actual setup appears in Figure 2. Because various wavelengths were utilized, the individual setups differed in the choice of laser and detector and their separation. However, Figures 1 and 2 are typical of the experimental setups used.

A Thompson Ramo Woolridge Model 71A Argon laser, providing 6 mw of average power at 60 pps, was used as the source of coherent radiation at .48μ. The beam was collimated to a diameter of 5.4 cm utilizing the mirror combination (see Figure 1) M_1, M_2, M_3 and had a uniform amplitude to within $\pm$ 1 db. The mirror system also served to direct the collimated beam to the appropriate target. The target is placed either on a stationary mirror mount or a platform capable of measuring aspect angles to $\pm$ 1/2 degree. The aspect angle was defined as the angle between the normal of the target surface and the bisector of the angle (~3°) between transmit and receive line of sight. The photodetector utilized was an RCA Model 7102 photomultiplier, with a spectral filter centered at .48μ, biased at -1100 volts dc and with a 1.1 cm aperture. The output of the photodetector was displayed on a Tektronix 585 oscilloscope using a 1A7 pre-amplifier.

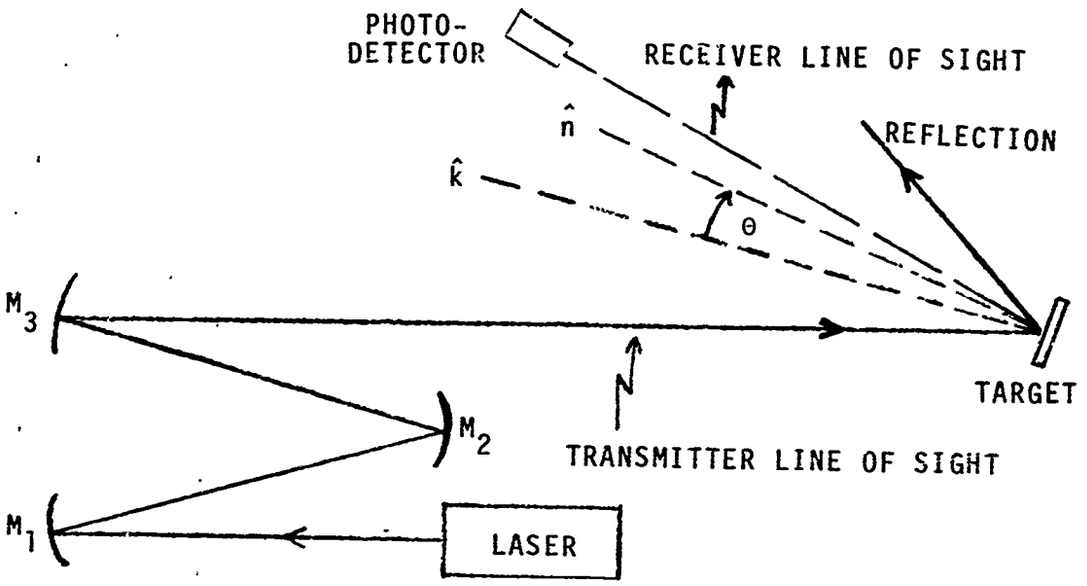

$\hat{k}$ ≡ BISECTOR OF TRANSMITTER AND RECEIVER LINE OF SIGHT

$\hat{n}$ ≡ NORMAL TO TARGET SURFACE

FIGURE 1

SCHEMATIC DIAGRAM OF REFLECTED POWER MEASURING SYSTEM

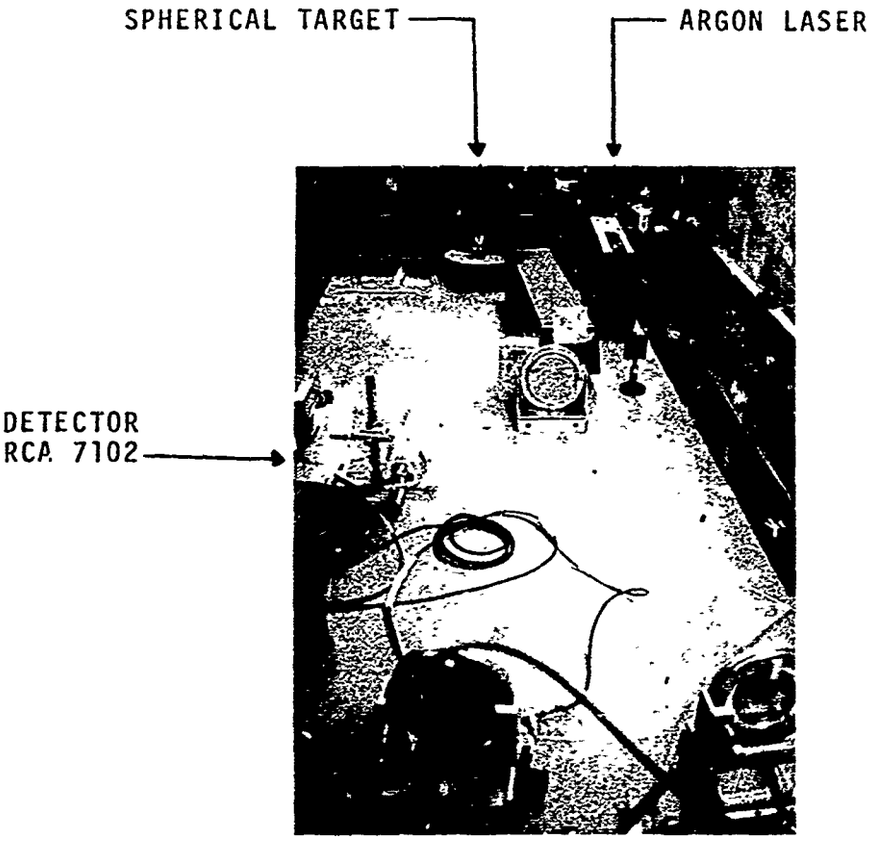

NOT REPRODUCIBLE

FIGURE 2

PHOTOGRAPH OF REFLECTED POWER MEASURING SYSTEM

A Spectra-Physics Model 120 HeNe laser, providing 5 mw cw power, was utilized as the coherent source for .63μ. To conveniently measure the reflected power and utilize the ac response of the detector to discriminate against noise, the .63μ beam was chopped at a rate of 4 kHz. Also, the beam was collimated to a diameter of 5 cm and was measured to be uniform to within ± 1 db over the 5 cm. The photodetector was the RCA 7102, with a spectral filter centered at .63μ, biased at 1300V dc and with a .95 cm aperture. A Tektronix 585 with the 1A7 was again utilized for measurements.

At 10μ, a Sylvania model 948 CO_2 laser, providing 5 watts cw, was used as the source. It also was chopped at 4 kHz in order to facilitate measuring the reflected signal amplitude. The beam was collimated to be uniform to within ± 1 db over 2.5 cm. The detector used, a Santa Barbara Au:Ge photoconductor, with an Irtran IV window and biased at 10V, had an effective aperture of .3 cm. The Tektronix 585 with the 1A7 was again utilized for data taking.

III. EXPERIMENTAL PROCEDURE

The experimental procedures followed in making the reflected power measurements will be discussed in this section. In addition, the data extraction process will be

presented. To a large extent what is said pertains to all wavelengths used.

As was presented earlier, both flat and spherical gold mirrors were utilized as targets. The choices were made because of their known radii of curvature, high degree of flatness, and approximately equal reflective properties at the three wavelengths. In addition, the 10 and 20 cm radii of curvature were chosen because of their resemblance to typical size spheres and other sharply convexed targets. The parameter which was measured in order to determine the relative reflective properties of these gold mirrors was simply the ratio of their respective reflected power. That is, the ratio of the response of a flat to both a 10 cm and a 20 cm mirror and the response of a 20 and a 10 cm mirror to each other were measured.

Another parameter dependent on the nature of a curved surface's power reflective capability is its Equivalent Flat Plate Radius (EFPR). EFPR is the radius of that circular area of a spherical surface which when illuminated by a plane wavefront is responsible for all of the reflected amplitude measured along the direction of the incident wavefront. The EFPR for both the 10 and 20 cm gold mirrors was measured simply by placing an aperture closely in front of the target,

of such a dimension that it decreased the measured reflected amplitude by 10%. The 10% was used to insure that the aperture indeed was superimposed on the circular area of the spherical surface responsible for the reflected amplitude.

In addition to the gold mirrors, two cylinders were also utilized as targets. This type of geometry was chosen because of its obvious resemblance to certain target vehicles. Each cylinder had a different finish in order to determine this effect on reflective characteristics. One cylinder was fabricated by simply wrapping silver foil around a cylindrical mold. This resulted in poor surface flatness and non-parallelism of the ends. The other cylinder was nickel plated, polished aluminum and fabricated to machine tolerances. In order to determine the effect of the target's cylindrical shape, finish, and form on its reflective properties, two characteristics were measured. The first was simply the ratio of reflected power for end-on and broadside incidences. The second was the reflected power pattern of amplitude versus aspect angle θ for a range of θ including end-on and broadside. The end-on and broadside returns were chosen for measurement because they yield data directly due to the differences in the radii of curvature between the cylinder's

flat and curved surfaces. In addition, the power pattern measurement should reveal any surface finish effects through departures from the expected specular peaked patterns.

To convert the reflected power characteristics of various surfaces to a LRCS value, it is necessary to compare it to the amplitude of the return from a standard target of known cross section. At optical wavelengths, a target's backscatter cross section is defined as that area of a Lambertian reflector which reflects as much power to the detector as the unknown surface.[2] A flame sprayed aluminum target, 30 cm X 30 cm X .32 cm was used as a standard.[3] It is the closest surface to a perfect Lambertian ($\cos\theta$ reflected power distribution) reflector available at 10μ. However, the only experimental arrangement which allowed detection of the reflected radiation from this standard target was the .48μ system. This was due to the inherently diffuse character of the target which reflected radiation to the detectors smaller than the minimum discernible signal (mds) except for .48μ. Therefore, the only target reflected power data which can be converted directly to cross section values is that at .48μ. The experimental data showed that substantial correlation does exist at all three wavelengths and is presented in Section V. Therefore, if it is assumed

that LRCS is not wavelength dependent from .48 - 10.6μ, we can determine a target's LRCS at .63 and 10.6μ by measurements at .48μ. Future experiments at the outdoor model range will corroborate this assumption by direct measurement of LRCS at .63 and 10.6μ.

The procedure used to determine experimental parameters such as the ratio of power returned from 20 cm versus 10 cm mirrors and the end-on versus broadside return from a cylinder will now be discussed. Essentially, the measurements at all wavelengths were made with the same display and recording equipment, a 585 Tektronix oscilloscope with a 1A7 pre-amplifier. The display was then recorded on film using a scope mounted camera. The data extraction will be for just .48μ with experimental results for the other wavelengths presented in Section V. The two amplitudes measured for various ratios were displayed on one oscilloscope picture by exposing one-half of the photographic film at a time. Since all the lasers used had some output variation in time, a number of trial runs were made for each amplitude comparison and averaged. An example of a trial run is displayed in Figure 3. This shows the reflected amplitude from a flat gold mirror on the left and the amplitude from a 10 cm gold mirror on the right. Figure 4 shows a trial run used

NOT REPRODUCIBLE

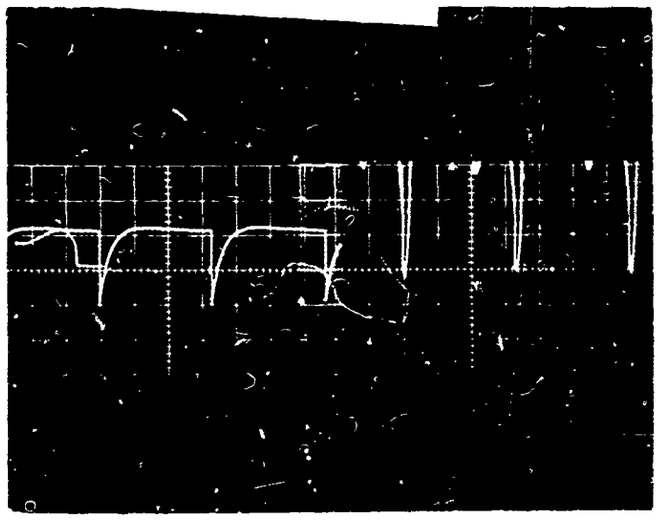

LEFT: 5mv/div vert.
5ms/div hor.

RIGHT: 10 μv/div vert.
5 ms/div hor.

FIGURE 3

PHOTOGRAPH OF THE REFLECTED AMPLITUDE FROM A FLAT GOLD MIRROR (LEFT) AND THE AMPLITUDE FROM A 10 cm GOLD MIRROR

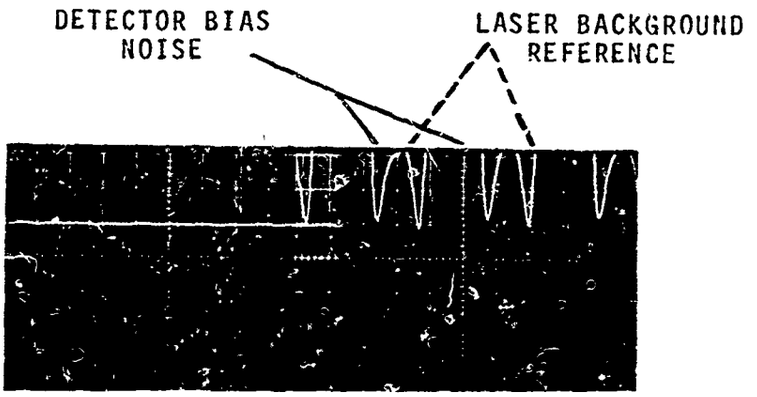

NOT REPRODUCIBLE

LEFT: 5mv/div vert.
5ms/div hor.

RIGHT: 10μv/div vert.
5ms/div hor.

FIGURE 4

PHOTOGRAPH OF BACKGROUND REFERENCE LEVELS FOR A FLAT MIRROR (LEFT) AND A 10cm MIRROR (RIGHT)

as a background reference level (target is removed from measurement setup) against which the amplitudes from various targets as in Figure 3 are compared. In Figure 4 the amplitude scale on the left is appropriate for flat surfaces and that on the right for curved ones. The trace on the right contains not only laser background reflections but also detector noise due to the bias supply which is readily discernable at these high gain pre-amplifier settings. Comparing the amplitude on the right in Figure 3 to its laser background reference in Figure 4, yields approximately 1 division. Further, comparing the amplitude on the left in Figure 3 to its background in Figure 4, yields approximately 2 divisions of amplitude. Taking into account the vertical scales in both traces (5mV/div on left, 10μV/div on the right), the ratio of left to right or flat to 10 cm mirror is 870. Succeeding photographs, Figures 5 and 6, show flat versus 20 cm and 20 cm versus 10 cm, respectively. These result in ratios of flat:20 cm and 20 cm:10cm of 230 and 3.9 respectively. Figure 7 shows the end-on incidence reflected amplitude on the left and broadside on the right for a cylinder, and resulted in a ratio of 390. As mentioned earlier, these traces are but a few among the many trials utilized to obtain an average amplitude value over a period of time large compared to any laser fluctuation period.

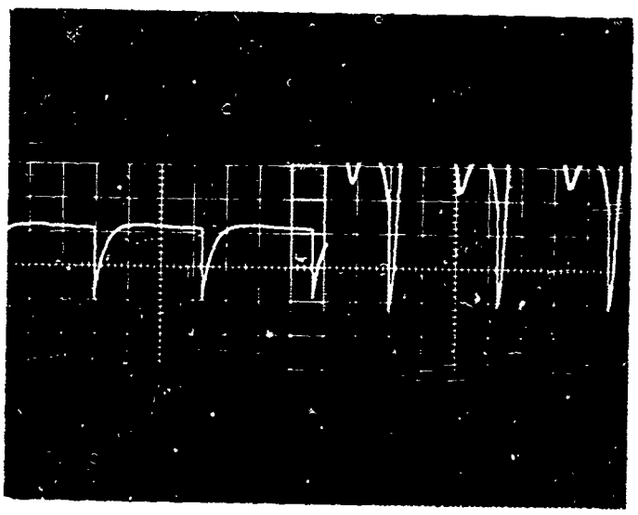

NOT REPRODUCIBLE

LEFT: 5mv/div vert. 5ms/div hor. RIGHT: 20μv/div vert. 5ms/div hor.

FIGURE 5

PHOTOGRAPH OF THE REFLECTED AMPLITUDE FROM A FLAT GOLD MIRROR (LEFT) AND THE AMPLITUDE FROM A 20cm GOLD MIRROR

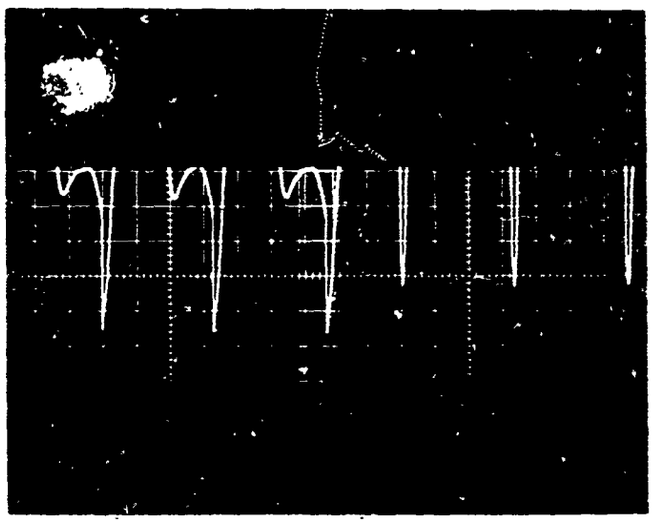

NOT REPRODUCIBLE

LEFT: 20μv/div vert. 5ms/div hor. RIGHT: 10μv/div vert. 5ms/div hor.

FIGURE 6.

PHOTOGRAPH OF THE REFLECTED AMPLITUDE FROM A 20cm GOLD MIRROR (LEFT) AND A 10cm GOLD MIRROR

NOT REPRODUCIBLE

LEFT: 5mv/div vert. 5ms/div hor. RIGHT: 10μv/div vert. 5ms/div hor.

FIGURE 7

PHOTOGRAPH OF THE REFLECTED AMPLITUDE FROM END ON INCIDENCE OF A CYLINDER (LEFT) AND BROAD SIDE INCIDENCE

IV. ANALYTICAL RELATIONSHIPS

Analytical expressions, to predict and verify experimental results, were empirically derived. The development of these expressions are discussed in this Section. Since we are only pursuing analytical estimates of various parameters, a rigorous theoretical treatise of LRCS phenomena would be beyond the scope of this report.

The first parameter to be measured was the ratio of reflected power from gold surfaces having various radii of curvature. The reflected power measured is directly proportional to the product of the power density incident on the gold surface and the area on the surface which reradiates power to the detector. Therefore, since the same uniform wavefront was used to illuminate all gold surfaces at a particular wavelength, the problem is reduced to the following. The ratio of reflected power from surfaces having two different radii of curvature is completely determined by computing the area on each gold mirror responsible for the radiation impinging on the detector. This area can be called an effective area (A_e). Figure 8 is a scattering diagram depicting the analytical terms and the important constraint that $Y + y = R_d$. This says the maximum value the radius of the reflected beam can have and still be

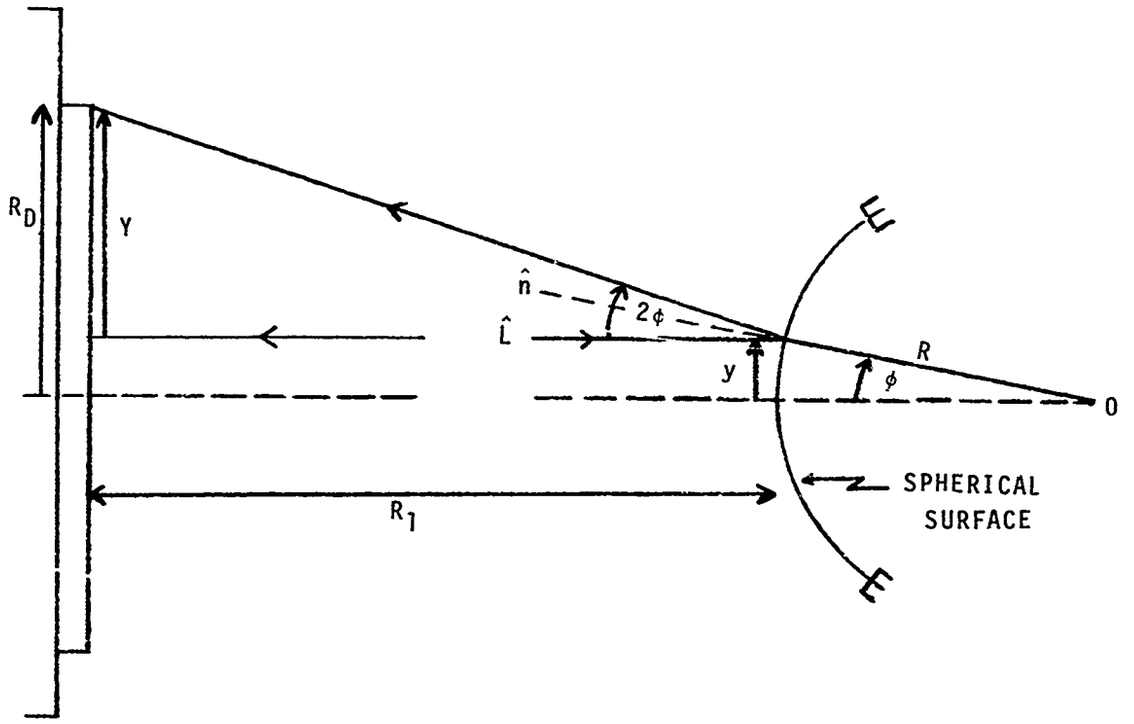

O ≡ CENTER OF RADIUS OF CURVATURE

$\hat{L}$ ≡ DIRECTION OF LASER LIGHT

$\hat{n}$ ≡ NORMAL TO SPHERICAL SURFACE

R ≡ RADIUS OF CURVATURE OF SPHERICAL SURFACE

R_1 ≡ RANGE FROM TARGET TO DETECTOR

R_D ≡ RADIUS OF DETECTOR APERTURE

y ≡ MAXIMUM RADIUS OF INCIDENT BEAM WHICH IS REFLECTED TO THE OUTER EDGE OF R_D.

Y+y ≡ RADIUS OF REFLECTED BEAM AT DETECTOR

FIGURE 8

DIAGRAM FOR THE ANALYSIS OF THE GEOMETRICAL OPTICS THEORY

detected by the receiving area of the detector is simply the radius of the detector aperture. From this we can work backwards to the spherical surface to determine A_e. Two assumptions are used in this derivation. The first is planar wavefront incidence on the target, and the second is that the theory of geometrical optics holds for the highly reflective metallic surface.

Since Y + y is the radius of the reflected beam at the detector, we need to know its value in terms of the experimental parameters R, R_D, and R_1 which describe the reflective surface, the detection medium, and the separation between the two, respectively. Therefore, let $\sin\phi = \frac{y}{R\cos\phi}$; for small ϕ, $\sin\phi \approx \phi \approx \frac{y}{R}$.

Also, $\tan 2\phi = \frac{Y}{R_1}$ and

again for small ϕ

$\tan 2\phi \approx 2\phi \approx \frac{Y}{R_1}$.

Therefore, $2\frac{y}{R} = \frac{Y}{R_1}$

or $Y = 2\frac{R_1}{R}\, y$.

However, $Y = R_D - y$.

Therefore, we have $y + 2y\frac{R_1}{R} = R_D$

$$\text{or } y = \frac{R_D R}{R + 2R_1} \quad . \qquad (1)$$

Equation (1) is the key expression, which is common to all further analytical estimates of reflected power ratios and EFPR. Again, it represents that dimension of a spherical surface of radius of curvature R responsible for the power impinging on a detector, at a distance R_1 away, with an aperture of radius R_D. It may be compared to another expression which describes that portion of a sphere which is responsible for reflected power in the direction of incident radiation. According to Barton,[4] a circular disc of radius $a_1 = \sqrt{\frac{a\lambda}{2\pi}}$ is that area of a sphere of radius a which is responsible for back scattered electromagnetic energy of wavelength λ in the direction of an incident plane wave-front. This expression does have a wavelength dependence and it will be interesting to compare its predictions for EFPR with those of Equation (1). To use Equation (1) and the effective area concept in determining the ratio of reflected power for curved surfaces of different radii, we proceed as follows. The power received at the detector is the product of the power density incident on the gold surface ρ_i and the surface's effective area A_e. A_e for a spherical

surface is just πy^2 or $\pi \left(\frac{R_D R}{R + 2 R_1}\right)^2$.

Therefore, the product $(\rho_i)\ (A_e) = \pi \left(\frac{R_D R}{R + 2 R_1}\right)^2 \rho_i$.

For surfaces of different radii i and j, illuminated by the same plane wavefront, the reflected power ratio R_p as measured by a common detector is simply:

$$R_p = A_{ei}/A_{ej} = \frac{R_i^2}{R_j^2} \left[\frac{R_j + 2R_1}{R_i + 2R_1}\right]^2 . \qquad (2)$$

For example, to find the ratio of a flat to 10 cm mirror, let $R_i = \infty$, R_j = 10 cm, and $R_i >> 2R_1$.

Therefore, R_p becomes $R_p = \left[1 + \frac{2R_1}{10}\right]^2$. (2a)

Similarly for a flat to 20 cm mirror R_p becomes $R_p =$

$$\left[1 + \frac{2R_1}{20}\right]^2 . \qquad (2b)$$

Lastly, for 20 to 10 cm mirrors R_p becomes $R_p =$

$$4 \left[\frac{10 + 2R_1}{20 + 2R_1}\right]^2 . \qquad (2c)$$

Equation (1) can also be used to determine the A_e of a cylinder at broadside when illuminated by a plane wave. The shape of A_e is an ellipse when the cylinder is viewed broadside as in Figure 8, with y as one semi-axis. In the

direction normal to y and the plane of Figure 8, the cylindrical surface is flat and, therefore, the maximum dimension which can be projected onto the detector is $2R_D$. Thus, R_D becomes the semi-axis perpendicular to y in a direction normal to the plane of Figure 8. Therefore, the broadside effective area A_e is simply $\pi y R_D$. At end on incidence, A_e is just the flat area projected onto the detector or πR_D^2. Therefore, the ratio of end-on A_e to broadside for a cylindrical shape results in a reflected power ratio R_p given by:

$$R = \frac{\pi R_D^2}{\pi y R_D} = \frac{R_D}{y} = \frac{R_D}{\frac{R_D R}{R + 2R_1}} = 1 + \frac{2R_1}{R} \quad . \qquad (3)$$

V. RESULTS

This section presents the data resulting from the experimental and analytical efforts discussed in previous sections.

Table 1 presents the results of the experimental measurements of the EFPR of 10 and 20 cm radii gold mirrors. Also included are analytical estimates based on Equation (1) and Barton's expression for wavelength dependent EFPR. It is obvious from Table 1 that the geometrical optics expression agrees more readily with experimental data at the shorter wavelengths (.48μ and .63μ) while the wavelength dependent

Wavelength Microns	10 cm Radius of Curvature Au Mirror			20 cm Radius of Curvature Au Mirror		
	Geometrical Optics (cm)	Barton's Theory (cm)	Experimental Results (cm)	Geometrical Optics (cm)	Barton's Theory (cm)	Experimental Results (cm)
.48	.0178	.0089	.0250	.0343	.0126	.0390
.63	.0350	.0100	.03505	.0685	.0139	.0575
10.6	.0040	.0400	.0435	.0086	.0564	.0625

T A B L E 1

EXPERIMENTAL AND THEORETICAL VALUES FOR EFPR
USING BOTH 10 CM AND 20 CM RADII OF CURVATURE GOLD MIRRORS

expression of Barton finds more agreement with the long wavelength (10.6μ) measurements. In addition, at a given wavelength, experimental measurements and both analytical expressions agree that the EFPR increases with increasing radii of curavature as it obviously should. Also, the experimental data and Barton's expression have EFPR increasing for a given mirror as the wavelength increases, in agreement with the concept that a given surface, in general, appears flatter at longer wavelengths. That is, a surface's roughness scale, which is the ratio of surface height fluctuation to wavelength (ℓ/λ), decreases for increasing wavelength.

Table 2 shows the results of the measurements of the ratio of reflected power from flat and spherical gold mirrors at .48μ, .63μ, and 10.6μ. The experimental numbers were arrived at by the method outlined in Section III, while the analytically determined ratio was calculated using Equation (2). The data shows substantial agreement between experimental and analytical values. In addition, within each wavelength, the 20 vs 10 cm experimental value obtained by direct measurement is substantially the same value which can be inferred when these mirrors are compared to a third. Further, the variation in the ratio of a given mirror configuration, as a function of wavelength, can be accounted

Wavelength Microns	Flat Au Mirror vs 10 cm Radius of Curvature Au Mirror		Flat Au Mirror vs 20 cm Radius of Curvature Au Mirror		20 cm vs 10 cm Radii of Curvature Au Mirrors	
	Theoretical Ratio (DB)	Experimental Ratio (DB)	Theoretical Ratio (DB)	Experimental Ratio (DB)	Theoretical Ratio (DB)	Experimental Ratio (DB)
.48	29.83	29.54	24.08	23.6	5.80	6.02
.63	31.40	30.4	25.58	25.2	5.80	5.19
10.6	29.14	28.4	23.71	22.7	5.80	5.74

TABLE 2

EXPERIMENTAL AND THEORETICAL RATIOS OF THE REFLECTED POWER FROM A FLAT AND TWO CONVEX GOLD MIRRORS

fr· y the use of different ranges for these wavelengths rather than any wavelength dependent phenomena.

In Table 3, an analytical estimate of reflected power, based on an assumption of specular scattering at end-on and broadside incidence, is compared to experimental data on a nickel plated 2 cm by 2 cm machined cylinder. While this same measurement was performed on a silver foiled, poorly formed cylinder for comparison, a reflected power pattern was measured for both cylinders with the aspect angle varied from end-on (0°) to broadside (90°). This pattern is plotted in Figures 9, 10, and 11 for .48, .63, and 10.6μ wavelengths, respectively. As is evident from these figures, the nickel plated cylinder pattern is always characterized by two spiked maxima. These so-called "speculars," have been shaded in to emphasize their being smaller than the angular width of the silver cylinder's maxima. Exactly how much smaller is not known because the aspect angle could only be measured to $\pm$ .5 degrees. However, the angle measurement was sufficient to indicate the width of the silver cylinder's maxima, and this is what distinguished the behavior of the two cylinders at all three wavelengths. Again, the major feature in each of these plots is the existence of a lobe width, about the end-on (0°) and broadside (90°) points for the poorly formed cylinder, greater than that of the nickel plated one.

Wavelength Microns	Experimental Ratio (DB)	Theoretical Ratio (DB)
.48	24.96	24.77
.63	24.64	24.77
10.6	25.02	24.77

T A B L E 3.

EXPERIMENTAL AND THEORETICAL VALUES OF THE END-ON VS BROADSIDE RATIO OF THE REFLECTED POWER FROM A CYLINDER

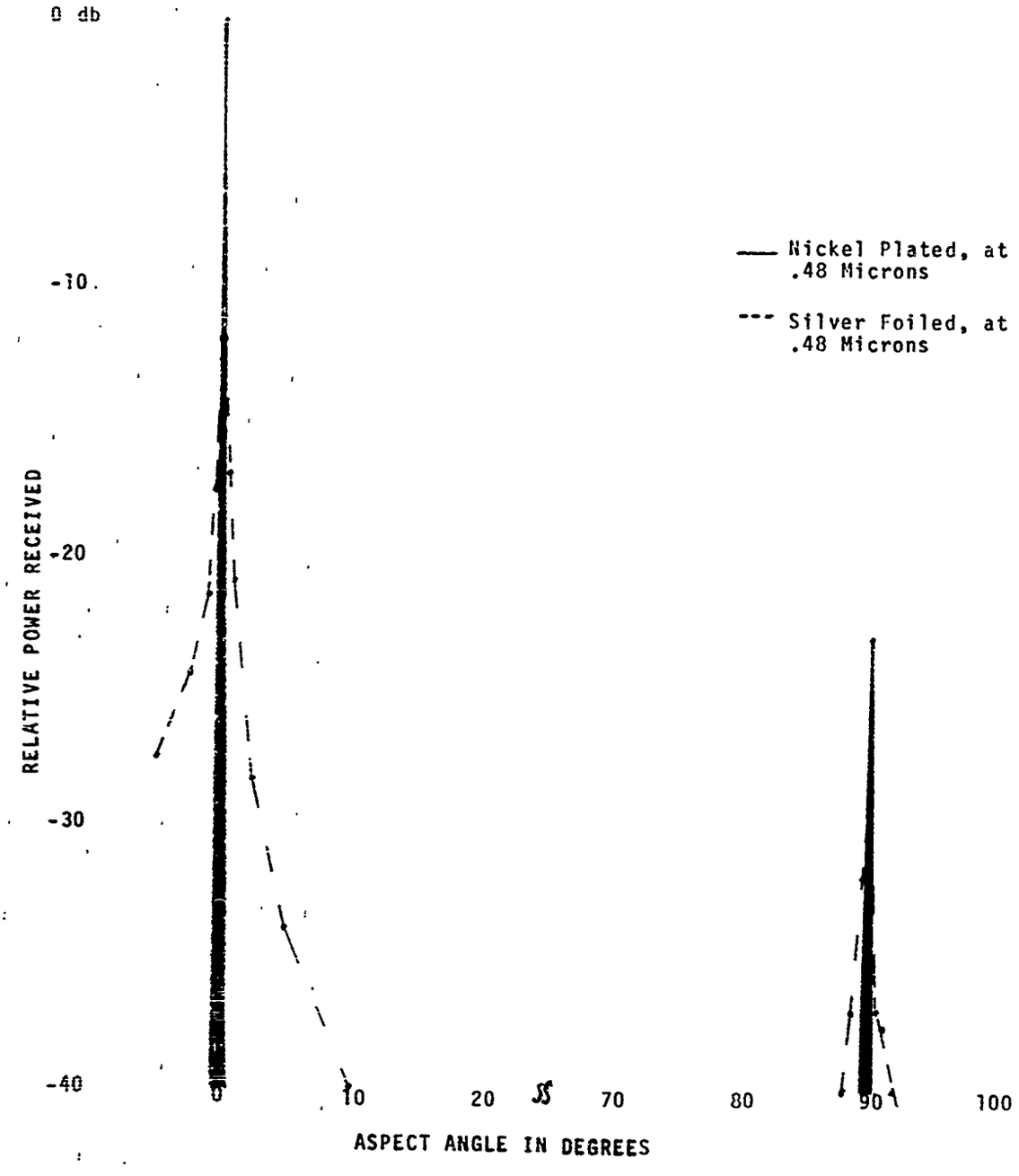

FIGURE 9

REFLECTED POWER PATTERN OF TWO CYLINDERS
USING .48 MICRON RADIATION

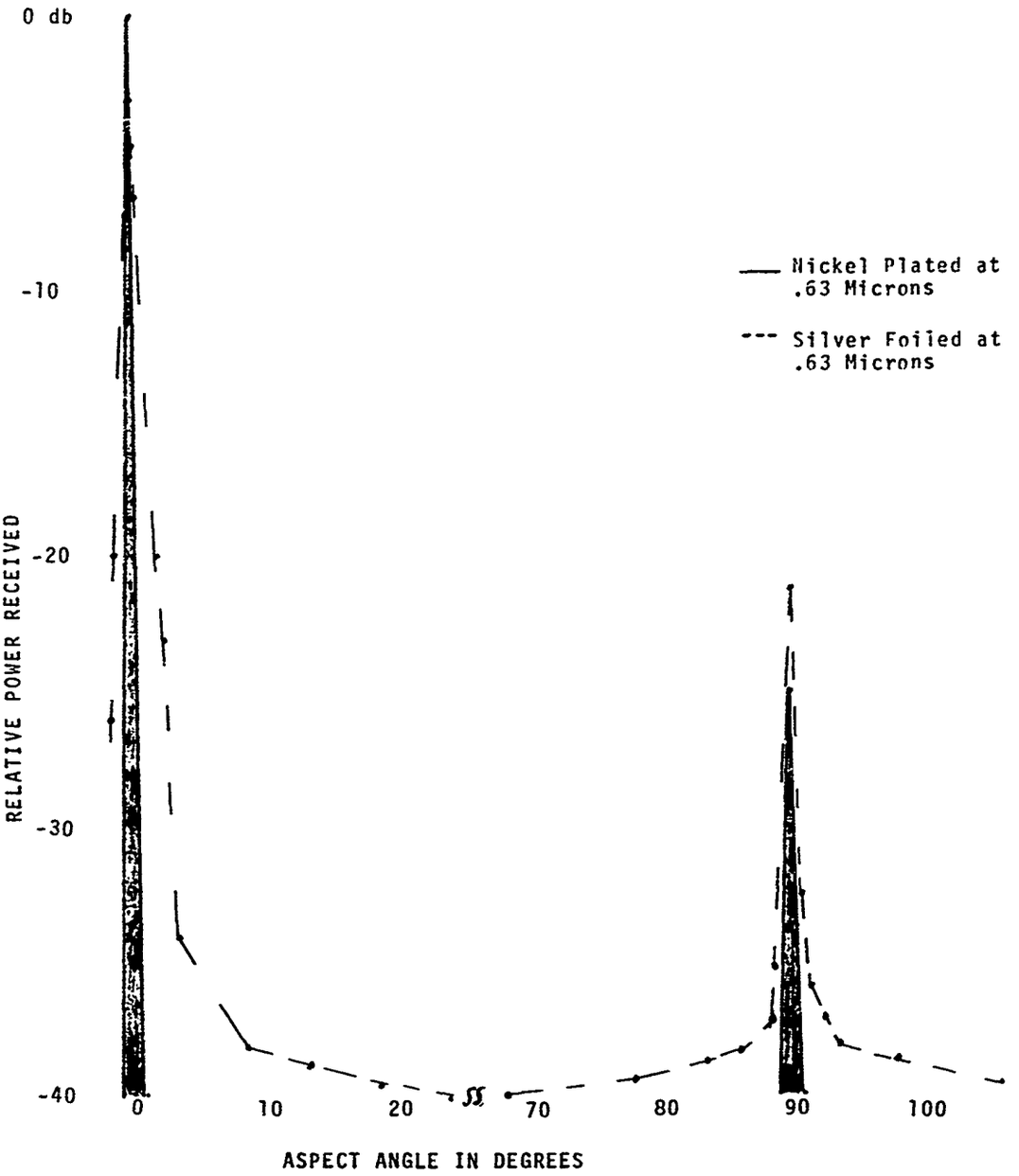

FIGURE 10

REFLECTED POWER PATTERN OF TWO CYLINDERS
USING .63 MICRON RADIATION

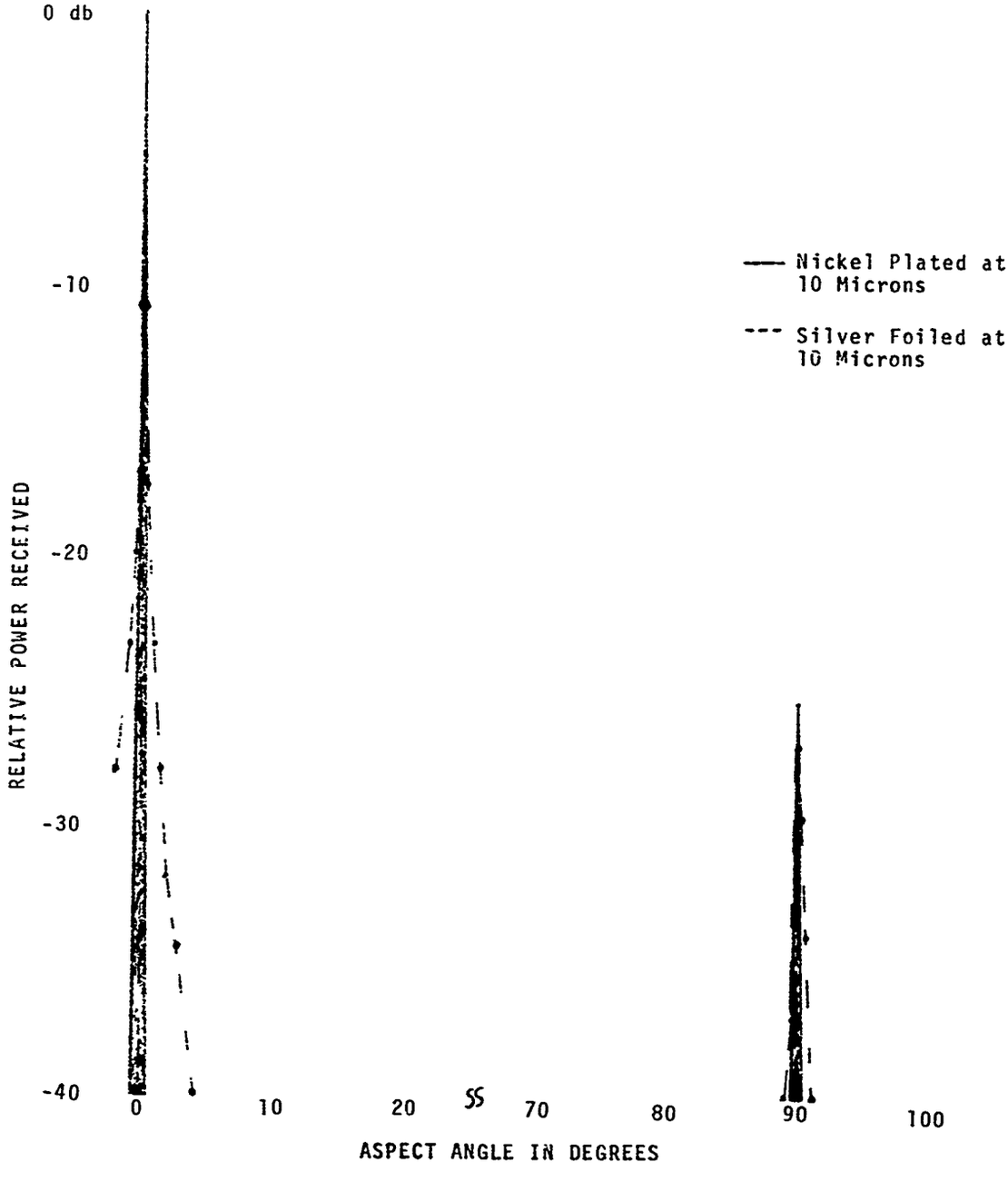

FIGURE 11

REFLECTED POWER PATTERN OF TWO CYLINDERS USING 10 MICRON RADIATION

In addition, the lobe widths appear to decrease as the illuminating wavelength increases. If the lobe width is indeed due to a roughness effect (ℓ/λ), it also would follow that as the illuminating wavelength becomes longer, this effect would decrease as shown in the experimental plots.

As stated in Section III, to convert the reflective characteristics of the various surfaces to LRCS values, it is necessary to calibrate the amplitude of the return against the return from a standard target of known cross section. A portion of the standard Lambertian target, equal in area to the incident beam (5.4 cm diameter) used in the reflective power measurements at .48μ, was illuminated in place of the metallic surfaces. The measured reflected amplitude was 6μv. This then calibrated the .48μ experimental set-up with a value of 6μv corresponding to a target cross section of 23 cm^2, the area of the illuminated standard target. Therefore, the cross section of any target in the .48μ set-up can now be determined by simply measuring its reflected amplitude and multiplying it by $\frac{23\ cm^2}{6\mu v}$. This was done for various surfaces at .48μ and the results are shown in Table 4. When the target was illuminated by the other wavelengths (.63μ and 10μ) no signal was detected at the receivers due to the minimum discernible signal of the detection system being

Target	Reflected Amplitude	LRCS $(CM)^2$
Flat Au Mirror	10 mV	1.7×10^3
10 cm radius of curvature Au Mirror	12 μV	46
20 cm radius of curvature Au Mirror	47 μV	180
Ni Cylinder viewed from end on	10 mV	1.7×10^3
Ni Cylinder viewed from broadside	30 μV	115

T A B L E 4

LRCS VALUES OBTAINED BY DIRECT CALIBRATION FROM A STANDARD LAMBERTIAN REFLECTOR USING 0.48μ RADIATION

greater than the small amount of scattered radiation from the Lambertian Scatterer. Therefore, cross-section values for the various surfaces at .63 and 10.6μ cannot be determined as yet by direct calibration from the standard Lambertian target. In future experiments at the Coherent Optical Radar Laboratory (CORAL) outdoor model range, LRCS wavelength dependence will be investigated by direct calibration of targets at .63 and 10μ by using the standard target and higher power sources to increase S/N at the receiver. In addition, an antenna pedestal positioner/recorder will be used for reflected power pattern measurements to improve angle resolution and read out.

VI. CONCLUSION

The effect of target surface and shape on the power reflected from it, as a function of aspect angle θ has been investigated at .48μ, .63μ, and 10.6μ, in a laboratory environment. In particular, at .48μ the reflected wave amplitude was measured relative to a standard cross-section target, a Lambertian Reflector. This enabled the determination of actual LRCS values for these targets at this wavelength. Based on a close examination of the experimental data resulting from three different wavelengths illuminating a common set of targets, any wavelength dependence correlated

very well with accepted simple roughness scale approximations to specular scattering theory. These approximations become important if it is necessary to extrapolate LRCS values from one wavelength to another. Further, to eliminate the necessity of extrapolating LRCS values from one wavelength to another, experiments are being implemented at the CORAL model range to calibrate simple and complex targets as a function of wavelength. Any subsequent theoretical attempt to predict and explain the LRCS of complex targets will require a more vigorous approach to explaining wavelength dependence than the above simple roughness scale approximations.

The measurement of the ratios of the reflected power from flat, 10 cm, and 20 cm radii gold mirrors resulted in quantitative information on the relative divergence of these surfaces. For example, a 10 cm radius mirror was from 28.4 - 30.4 db more divergent than a flat, while a 20 cm mirror was from 22.7 - 25.2 db more divergent than the same flat.

The importance of target finish and quality upon an optical radar's return was demonstrated vididly by the comparison of the reflected power patterns of Ni and Ag cylinders at the three wavelengths. A definite distinction between the two cylinders in quality of fabrication became

all the more evident when certain features of the power patterns were definitely attributable to the roughness of the cylinder's appearance. In addition, the variation in amplitude (~25 db) which can be expected from a cylindrical shape as a function of θ was also evident from these plots.

The EFPR measurements of 10 cm and 20 cm radii Au surfaces showed that the effective reflective area is quite small (-50 db) compared to a fully illuminated spherical surface in a detection system measuring reflected power from that spherical surface.

This report concludes the laboratory LRCS measurements. However, it has furnished the background and experimental approach for an outdoor model measurements program at RADC's 10μ CORAL. This program will provide data on targets in the physical, illumination, and detection environment of the radar.

REFERENCES

1. Demma, F.J., Michels, J.H, "Doppler Measurements From Specular and Diffuse Targets, In Rotational and Translational Motion, Using .6 and 10.6 Radiation," RADC-TR-70-83, p1, May 1970.

2. Wyman, P. W., "Definition of Laser Radar Cross Section," Applied Optics, Vol. 7, p 207, Jan 1968.

3. Brandewie, K.A., et al, "Coherent Imaging and Moving Target Detection at 10 Microns (U)," AFAL-TR-69-360, p 92, Jun 1970.

4. Barton, D.K., "Radar System Analysis," (New Jersey: Prentice-Hall, Inc.), p 67, 1964.